J. Fluid Mech. (1995), *vol.* 298, *pp.* 249–269

On the kinematics of short waves in the presence of surface flows of larger scales

By A. RAMAMONJIARISOA

Institut de Recherche sur les Phénomènes Hors Equilibre, Laboratoire IOA, Case 903, 163, avenue de Luminy, 13288 Marseille, France

(Received 18 October 1994 and in revised form 13 April 1995)

When the resonance condition is satisfied, i.e. that the local group velocity of short surface waves matches the local velocity associated with a larger-scale surface flow, it is known that the short waves are reflected or trapped by the flow. A typical example is the case of short surface waves propagating on long surface waves. By direct numerical resolution of the kinematic equations, some aspects of the reflection or trapping are first examined. Next, the effects of a second long wave on the trajectory of the short waves are considered. It is found that the trajectory is strongly distorted in general. Reflection still occurs, having a larger effect on the variation of the short-wave wavenumber than when only a single long wave is present. The entrapment becomes more sporadic. At short time intervals, a forced Mathieu equation is found to govern the short-wave development. This leads to a discussion on a more general physical context.

1. Introduction

In recent years, the evolution of short surface waves on variable surface velocity fields, for instance due to a surface current or to a long wave, has been a topic of many papers. This increasing interest is particularly motivated by the need for proper interpretation of signals from microwave remote sensing devices used to detect surface or underwater motions or obstacles.

Theoretical work was initiated by Longuet-Higgins & Stewart (1960, 1961) and Bretherton & Garrett (1968). This was then extended by many authors with applications to specific fields (Basovich & Talanov 1977; Phillips 1981; Shyu & Phillips 1990; Henyey *et al.* 1988). Some aspects of these contributions were recalled in the recent paper of Trulsen & Mei (1993). One of the main results of the investigations (Phillips 1981; Shyu & Phillips 1990) is the blockage or reflection of the surface waves at the points where their group velocities balance the convection by the larger-scale flow.

In the works cited above, a single long wave was often considered. This constitutes clearly an ideal situation, not satisfied in many real conditions, and this motivated our works, which is devoted to a first step towards multiscale analysis. The work is limited to the kinematics aspects, the objective being to look at the blockage process when many scales are present. Actually, the case of a short-wave packet over two large-scale velocity fields is the main subject considered. This is done by direct numerical resolution of the kinematic equations. The case of a capillary–gravity wave over short gravity waves (Phillips 1981) is taken as basic example, but, as mentioned in the concluding remarks, the author believes that the results are of general interest.

The case of a single short wave over a single oscillatory surface velocity field is first

examined (§2). The blockage or reflection mechanism is of course confirmed but the roles of various parameters of the flows as well as the initial conditions are clarified. The main new results concern the case of a short-wave packet over two large-scale surface velocity fields (§3). This is followed by an attempt to develop approximate equations for the short-wave displacement (§4). A driven Mathieu equation is found to be an asymptotic form. Finally, some preliminary conclusions and suggestions for future work are presented (§5).

2. Short waves over one single oscillatory surface velocity field

Most previous work has been addressed to this simple situation. Detailed aspects of the short-wave trajectories will be considered herein by direct numerical solution of the kinematic equations.

As is well known, the presence of a surface current leads to a transformation of the short-wave dispersion relation, due to a Doppler frequency shift. The dispersion law now becomes

$$\omega(\boldsymbol{k}, \boldsymbol{x}, t) = \omega_0(\boldsymbol{k}) + \boldsymbol{k} \cdot \boldsymbol{U}(\boldsymbol{x}, t), \tag{1}$$

where x and t denote the horizontal coordinate and the time; $\boldsymbol{U}$ is the velocity at the water surface; ω and $\boldsymbol{k}$ are the short-wave frequency and wave vector; $\omega_0(\boldsymbol{k})$ is the short-wave dispersion law in the absence of the surface velocity.

Within the framework of the geometrical optics approximation, the kinematics of the short waves is governed by the so-called ray equations or Hamilton equations (see e.g. Basovich 1979):

$$\dot{\boldsymbol{x}} = \frac{\partial \omega(\boldsymbol{x}, \boldsymbol{k}, t)}{\partial \boldsymbol{k}}, \qquad \dot{\boldsymbol{k}} = -\frac{\partial \omega(\boldsymbol{x}, \boldsymbol{k}, t)}{\partial \boldsymbol{x}}. \tag{2a, b}$$

Note that these equations can be derived directly (Irvine 1987) from the usual conservation equations (see e.g. Phillips 1977). In the following, the analysis is limited to two-dimensional configurations.

As a first example, let us consider capillary–gravity waves over a surface current of the simple form

$$U(x, t) = U(x, t) = U_0 \cos(K_0 x - \Omega_0 t). \tag{3}$$

U is the surface current velocity, with amplitude, wavenumber and frequency U_0, K_0 and Ω_0 respectively.

Then, the capillary–gravity wave dispersion law can be written as

$$\omega(k, x, t) = \omega_0(k) + kU_0 \cos(K_0 x - \Omega_0 t), \tag{4}$$

with

$$\omega_0(k) = (gk + \gamma k^3)^{1/2}, \tag{5}$$

g being the acceleration due to gravity and γ the ratio of surface tension to water density. Equation (4) is a small-amplitude approximation for the dispersion of capillary waves over a long gravity wave (Sinitsyn, Leykin & Rozenberg 1973; Phillips 1981). In this case $U_0 = \epsilon_0 C_0$, with $C_0 = \Omega_0 / K_0$ the phase celerity of the long wave with wave steepness ϵ_0.

In a frame of reference moving at C_0, the kinematic equations are

$$\dot{x} = \left(\frac{g}{k} + \gamma k\right)^{1/2} \left(\frac{1}{2} + \frac{\gamma k}{g/k + \gamma k}\right) + \epsilon_0 C_0 \cos K_0 x - C_0, \tag{6a}$$

$$\dot{k} = k \epsilon_0 \Omega_0 \sin K_0 x. \tag{6b}$$

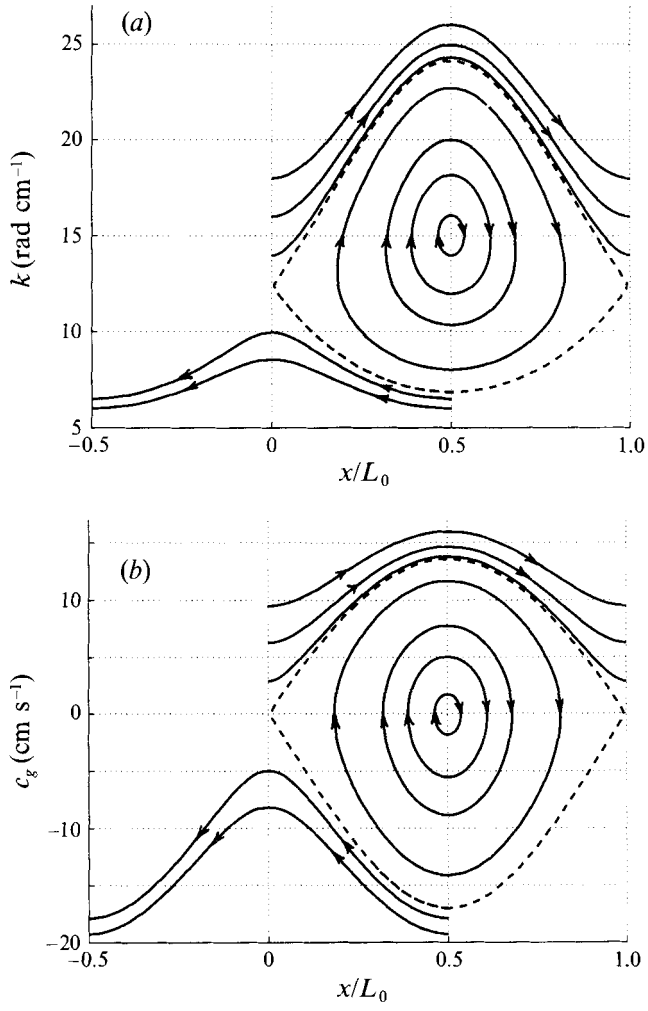

FIGURE 1. (*a*) ——, Examples of WKB phase-space trajectories of capillary–gravity wave packets in the field of a single long gravity wave of wavenumber $K_0 = 0.44$ rad cm^{-1} (wavelength $L_0 = 14.279$ cm) and wave steepness $\epsilon_0 = 0.05$; – – –, separatrix between trapped and untrapped short waves. The arrows indicate the short-wave displacement direction. (*b*) Velocity–position phase-space trajectories corresponding to (*a*).

The solution of (6) obviously depends upon the initial ($t = 0$) values of the short-wave wavenumber and position, respectively denoted k_0 and x_0. From the work of Phillips (1981), blockage or reflection of the capillary–gravity waves is expected over short gravity waves (wavelength of order 10 cm). This can be anticipated, as seen from the linear dispersion relation.

Solutions of (6) were found numerically by using a Runge–Kutta order 4–5 scheme with k_0 ranging from 6 to 25 rad cm^{-1} while x_0 varies from 0 to half the long-wave wavelength. The respective values of K_0 and ϵ_0 were 0.44 rad cm^{-1} ($L_0 = 14.279$ cm) and 0.05. The results were plotted in terms of trajectories in the (x, k) phase space, the so-called WKB phase space.

Figure 1 displays the trajectories for various initial positions and wavenumbers. Clearly, depending upon x_0, the wavenumbers within a certain domain correspond to closed orbits.

The width of the entrapment zone so defined increases when x_0 increases from 0 to $L_0/2$ and then decreases in a symmetrical way. Clearly, the determination of the entrapment domains is of interest. This requires the determination of the separatrix.

For the present simple situation of a short-wave packet over a single current with phase celerity C_0, the current is stationary in the frame of reference moving at C_0. Then, the dispersion relation

$$(gk+\gamma k^3)^{1/2}+kC_0(\epsilon_0\cos K_0 x-1)=f \tag{7}$$

gives a first integral of equation (1); f is the frequency in the moving frame of reference. Instead of solving the system (6), Basovich & Bahanov (1984) used this property to construct trajectories of short gravity waves in the (x,k) phase space.

Note that f_0, the initial frequency corresponding to initial wavenumber k_0 at initial position x_0, is

$$f_0=(gk_0+\gamma k_0^3)^{1/2}+k_0 C_0(\epsilon_0\cos K_0 x_0-1). \tag{8}$$

The frequency being constant, the dispersion relation (7) gives

$$k^3-\gamma^{-1}C_0^2(\epsilon_0\cos K_0 x-1)^2k^2+k\gamma^{-1}[g+2f_0 C_0(\epsilon_0\cos K_0 x-1)]-\gamma^{-1}f_0^2=0. \tag{9}$$

Examination of the trajectories displayed on figure 1 clearly suggests that saddles points are located at the crests of the long wave ($x=0$ or $2\pi/K_0$). Then, at given x_0, the separatrix is determined by looking, from (9), for values of k_0 yielding to two equal real roots at $x=0$ or $x=2\pi/K_0$. With

$$\left.\begin{aligned} &a_0=-f_0^2\gamma^{-1},\\ &a_1=[g+(2U_0 f_0)]\gamma^{-1}; \quad U_0=C_0(\epsilon_0\cos K_0 x-1),\\ &a_2=-U_0^2\gamma^{-1},\\ &q=\tfrac{1}{3}a_1-\tfrac{1}{9}a_2^2, \qquad r=\tfrac{1}{6}(a_1 a_2-3a_0)-\tfrac{1}{27}a_2^3, \end{aligned}\right\} \tag{10}$$

two real roots are known to exist if

$$s=q^3+r^2=0. \tag{11}$$

Then, k_0 corresponding to separatrix is a root of (11). The roots, in principle, can be found analytically, through lengthy algebra. Here, they were determined numerically. The separatrix is displayed on figure 1 (*a*).

Figure 1 (*b*) shows the trajectories of the short-wave packets using the conventional velocity (c_g)–position phase space. It is seen that except for packets exhibiting small variations of position and velocity (or wavenumber), the so-called 'well-trapped' packets, there is no complete similarity between the wavenumber and the velocity variations. This limits the analogy between this problem and the motion for an electron in the field of a plasma wave, as shown by Basovich (1979), to only the well-trapped short-wave packets.

From Basovich & Bahanov (1984), it is known that the width of the entrapment zone increases with the ratio between the surface current velocity amplitude and phase celerity. To specify this in a little more detail for the present situation, trajectories of capillary waves in a surface velocity field associated with a Stokes wave at moderate steepness were determined. This was done on the basis of the approximation which arises from the experimental investigation of Melville & Rapp (1988) showing that for a wave steepness up to 0.23, the horizontal velocity $u(x,\eta,t)$ at the surface is reasonably predicted by the formula

$$u(x,\eta,t)\approx\omega\eta(x,t), \tag{12}$$

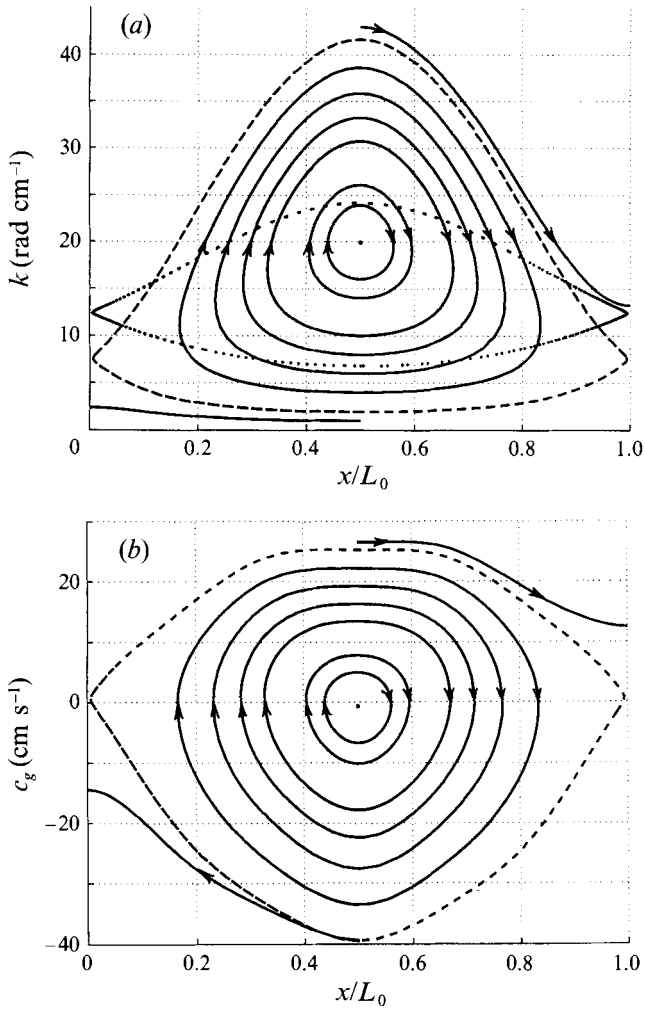

FIGURE 2. ——, As figure 1(*a*) but with $\epsilon_0 = 0.23$; ..., separatrix at $\epsilon_0 = 0.05$; – – –, separatrix at $\epsilon_0 = 0.23$. (*b*) Velocity–position phase-space trajectories corresponding to (*a*).

where $\eta(x, t)$ is the surface displacement and ω the frequency of the wave. With the above value of the steepness of the Stokes wave (wavenumber $K = 0.55$ rad cm^{-1}), figure 2 illustrates the trajectories of capillary–gravity waves in the (k, x) and (c_g, x) phase spaces. Again, it is seen that similar trajectories in both spaces exist only for the well-trapped short-wave packets. As shown on figure 2(*a*), the entrapment zone is indeed much larger at $\epsilon_0 = 0.23$ than at $\epsilon_0 = 0.05$.

Phillips (1981) showed that the situations above are of interest for interpreting observational results in laboratory facilities. In a field situation, blockage or reflection of short waves is also possible in the presence of a surface current due to internal waves, as illustrated by figure 3. The surface current velocity is taken to be of the form

$$u_i = U_i \operatorname{sech}^2 K_i(x - C_i t), \tag{13}$$

which is a satisfactory representation of the evolution observed, for example, during the SARSEX campaign (see Gasparovic, Apel & Kasischke 1988). The wavenumber K_i and the celerity C_i were chosen from among the values observed during this campaign, namely, $K_i = 0.017$ rad m^{-1} ($L_i \approx 370$ m) and $C_i = 0.76$ m s^{-1}.

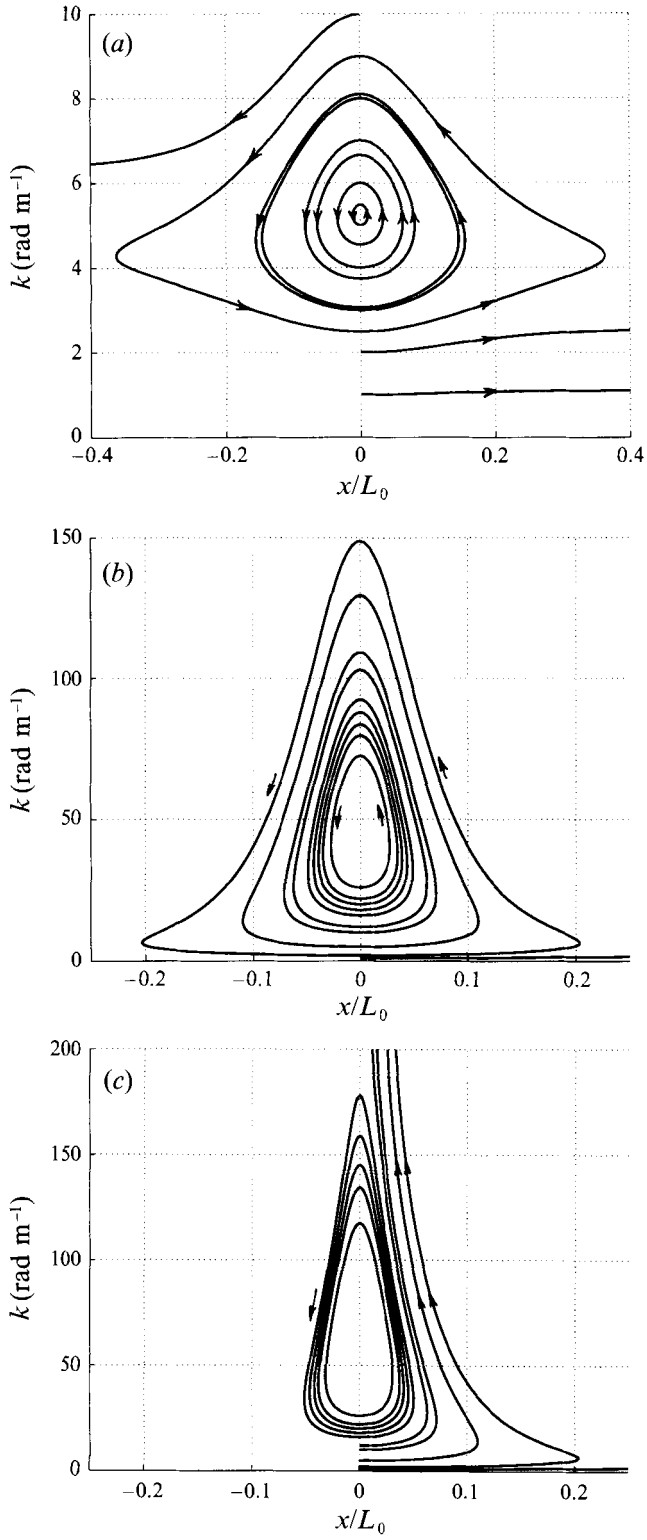

FIGURE 3. For caption see facing page.

To stress the importance of the ratio $\beta_i = U_i/C_i$ on not only the width of the entrapment zone but also on the wavenumber modulation, two different values of β_i were chosen. For $\beta_i = 0.10$, it is seen (figure 3*a*) that waves in the 1 m wavelength range (wavenumber in the range 3 to 9 rad m^{-1}) are trapped by the current. The wavenumber modulation remains small in the sense that the wavelength stays in the 1 m range. Inclusion of surface tension terms in the kinematic equations does not lead to a significant change in the results.

From figure 3(*b*), at a higher value of β_i, that is $\beta_i = 0.69$ which corresponds to values observed during SARSEX, the entrapment zone is increased considerably, now including wavenumbers in the range 2 to 26 rad m^{-1}. The wavenumber modulation is also considerably increased so that an initial wave in the 1 m wavelength range can be reflected as extremely short capillary waves. Figure 3(*b*) corresponds to the case where the surface tension terms are neglected in the ray equations. Including these terms dramatically increases the wavenumber modulation (figure 3*c*): all waves in the entrapment zone are now reflected as extremely short capillary waves.

3. Kinematics of the short waves in the presence of two oscillatory surface velocity fields

The simplest situation of a single short-wave packet over a single oscillatory surface current or long wave treated above and also by many other authors is possibly unrealistic in many respects. In particular, in practical situations, many short-wave components and long-wave or surface current components are often present.

The corresponding general problem would be extremely complicated to analyse. As a first step to consideration of realistic situations, the kinematics of a single short-wave packet over two long waves or oscillatory currents are studied in what follows.

Sinusoidal currents with respective wavenumbers K_0 and K, phase celerities C_0 and C, and amplitudes $\beta_0 C_0$ and βC are considered.

The dispersion relation of capillary–gravity waves in the field of these currents is now

$$\omega(k, x, t) = (gk + \gamma k^3)^{1/2} + k\{\beta_0 C_0 \cos K_0(x - C_0 t) + \beta C \cos[K(x - Ct) + \psi]\}. \quad (14)$$

The two constants β_0 and β are usually less than unity and ψ is a constant phase difference between the two currents. We shall be mostly interested in the influence of a second current on the trajectories of short waves originally trapped by the 'basic' current labelled '0'. Then, it is natural to transform to a frame of reference moving with the phase velocity C_0. In this frame, the kinematic equations can be written as

$$\dot{x} = \left(\frac{g}{k} + \gamma k\right)^{1/2}\left(\frac{1}{2} + \frac{\gamma k}{g/k + \gamma k}\right) + \beta_0 C_0 \cos K_0 x + \beta C \cos(Kx + \delta\Omega_0 t + \psi) - C_0, \quad (15a)$$

$$\dot{k} = k[\beta_0 \Omega_0 \sin K_0 x + \beta\Omega \sin(Kx + \delta\Omega_0 t + \psi)], \quad (15b)$$

with $\delta = K/K_0 - \Omega/\Omega_0$, $\Omega_0 = C_0 K_0$, $\Omega = CK$; $(\delta\Omega_0)^{-1}$, which represents the time interval (the 'autocorrelation time') between two successive patterns of constructive or destructive interference of the current variations, plays a crucial role in the short-wave evolution. We would expect the evolution at small δ (currents with closely similar

FIGURE 3. Examples of WKB phase-space trajectories of capillary–gravity and short gravity waves in the field of an internal-wave-induced surface current (amplitude U_i, phase velocity C_i): (*a*) $U_i/C_i = 0.10$, identical results with and without surface tension; (*b*) $U_i/C_i = 0.69$, surface tension ignored; (*c*) $U_i/C_i = 0.69$, surface tension included.

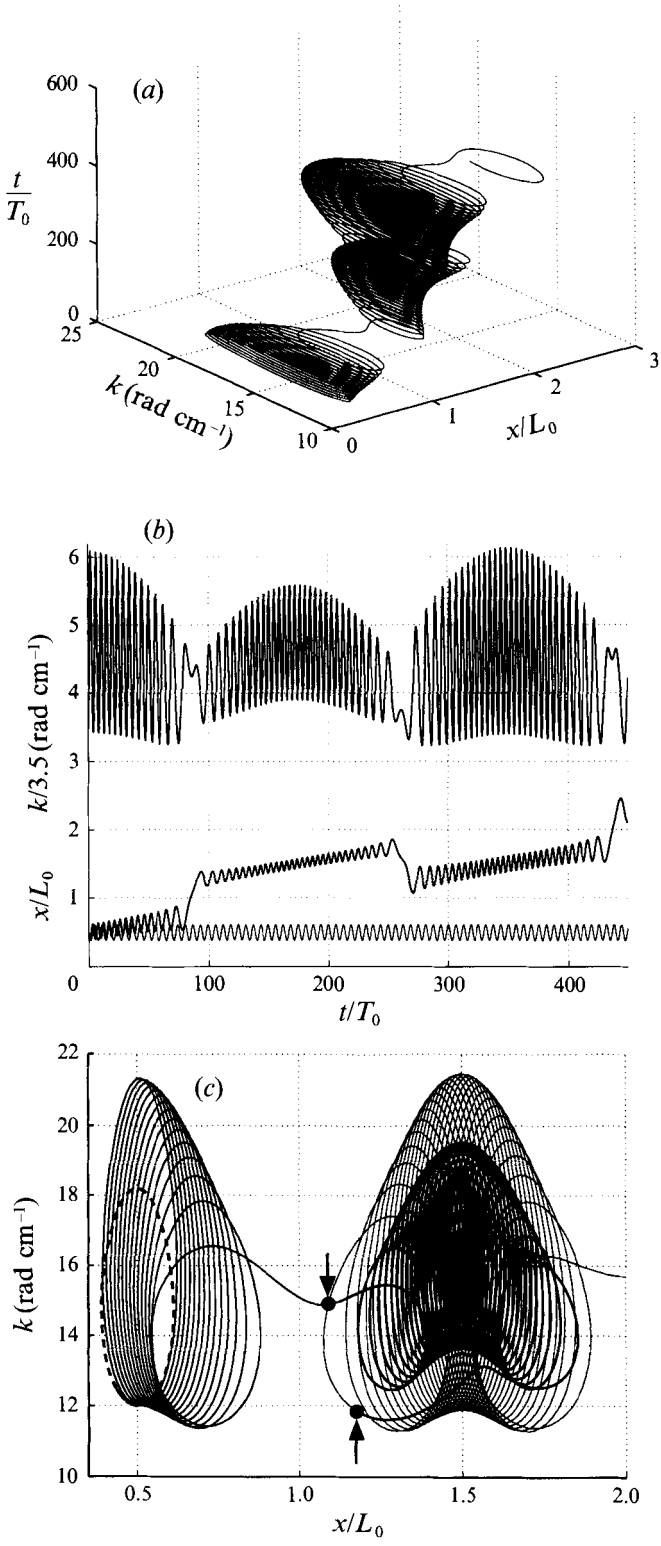

FIGURE 4. (*a*) Three-dimensional phase portrait of a capillary–gravity wave with initial wavenumber k_0 in the field of two long gravity waves. (*b*, *c*) Two-dimensional projections: (*b*) in the time–

characteristics) to significantly differ from the evolution at large δ (currents with well separated characteristics). We will first illustrate this before doing a more detailed approximate analytical study.

According to results for a single current, K_0 was taken as 0.44 rad cm^{-1}. To have a small value of δ, K was taken as 0.435 rad cm^{-1}. Then $\delta \approx 0.0057$ and $1/\delta \approx 176$. Here, as well as in the next examples, values of C_0, C, Ω_0 and Ω were determined by applying the linear dispersion relation for a gravity wave. β_0 and β were taken as 0.05. Then, again, we are looking at approximate models of the kinematics of capillary–gravity waves in the orbital velocity fields of two gravity waves.

Figure 4 shows the three-dimensional phase portrait and the two-dimensional projections in various planes with the initial wavenumber $k_0 = 12$ rad cm^{-1}. From figure 4(*b*), the time interval which separates two successive complete interference patterns in the time evolution of the short-wave position and wavenumber is found to be about $173T_0$, T_0 being the period of the 'basic' gravity wave. Then, the computed value δ_c of δ is such that $1/\delta_c \approx 173$, which is a value very close to the theoretical value given above. As expected, other computations showed no dependence of the computed δ_c on either the initial wavenumber or the initial position.

Figure 4(*c*) displays the short-wave trajectories in the WKB phase space. The closed orbit when a single long wave is present is also shown for comparison. With two long waves present, the trajectories are no longer closed: the short-wave packet exhibits orbital motions around a point which moves slowly away from the trough of the basic long wave. Finally, after a number of cycles, it jumps to the next trough to be trapped there during two successive separated time intervals T_0/δ. In detail, as shown, there are three different families of trajectories corresponding to the three time intervals above. By extending the computation to larger time intervals, no repetition of the patterns was found.

It is of interest to note that the wavenumber modulation is significantly larger with two long waves than with one single long wave. This would be related to the modulation of the surface current amplitude. In practice, the dissipation effect by viscosity would be more effective with two long waves.

Other computations made with $\delta^{-1} = 88$ and $\delta^{-1} = 27$ confirm the previous result on the role of this parameter and the presence of wavenumber modulation larger than in the case of a single long wave. Depending upon δ, the short-wave packet undergoes many or few bounces in the trough of the basic wave before leaving this trough to move to the next ones. The detailed patterns in the WKB phase space change very significantly with δ and cannot be predicted without carrying out a complete computation.

The example above suggests that, if δ is sufficiently high, i.e. K_0 and K depart significantly from another, the blockage effect would rapidly disappear. This is confirmed by the computational results at $K_0 = 0.44$ rad cm^{-1} and $K = 0.31$ rad cm^{-1}: δ^{-1} is then of order of 7.

Figure 5, which corresponds to the initial value of the short-wave wavenumber $k_0 = 12$ rad cm^{-1} at the initial position $x_0 = L_0/2$, illustrates some main features of the results.

As in figure 4(*a*), the three-dimensional phase portrait is shown on figure 5(*a*).

wavenumber plane (upper curve), in the time–position plane (lower curves), and (*c*) in the WKB plane. Trajectories in the presence of a single long wave are also shown as light line on (*b*) and broken line on (*c*). The three parts of the trajectories seen in (*c*) correspond to successive time intervals: $0 < t/T_0 \leqslant 75$ (heavy line); $75 \leqslant t/T_0 \leqslant 230$ (very heavy line); $75 \leqslant t/T_0 \leqslant 230$ (light line). The limits of the intervals are shown by small arrows. $\delta = 1/176$; $k_0 = 12$ rad cm^{-1}; $x_0 = L_0/2$; $b_0 = b = 0.05$.

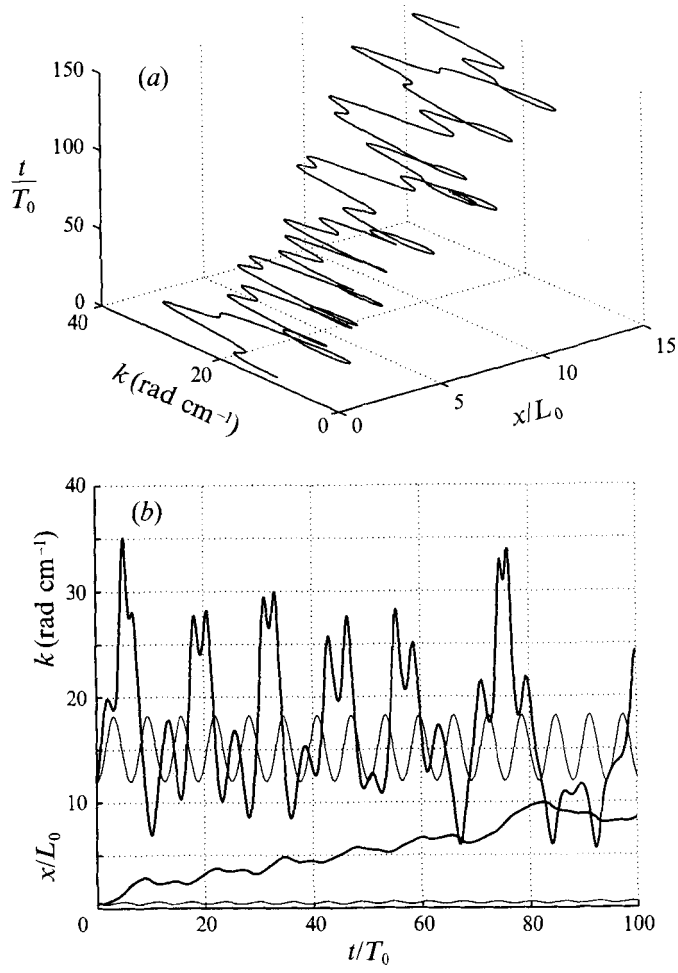

FIGURE 5(*a*, *b*). As figures 4(*a*) and 4(*b*) but with $\delta = 1/7$.

Figure 5(*b*) shows the displacement with respect to the time the short wave leaves its initial position, moves to the next trough to be trapped there for a certain amount of time t_e, moves to the next trough to be trapped again and so on.

The entrapment time interval t_e is found to be of order $10T_0$ which agrees in order of magnitude with the theoretical value of $(\delta\Omega_0)^{-1}$. During the entrapment time intervals, the wavenumber exhibits quite similar evolutions (figure 5*b*). Such similarity is also noticeable in the WKB phase-space trajectory (figure 6*a*). However, in detail, no fully repetitive pattern can be found in these evolutions and trajectories. In fact, as shown on figure 6, there is a large variety of trajectories depending in particular upon the initial value of the short-wave wavenumber. Clearly, again, these trajectories cannot be predicted *a priori*, without carrying out a complete numerical computation.

While no energy consideration is made here, the following preliminary comments are of interest concerning the specific practical examples above. For capillary–gravity or capillary waves the reflection as extremely short capillary waves would lead to a rapid dissipation by viscosity. Then, the waves would disappear almost instantly. However, in the presence of wind, this conclusion may be not valid. Indeed, using a very sophisticated visualization technique, able to resolve capillary waves down to $\frac{1}{3}$ mm

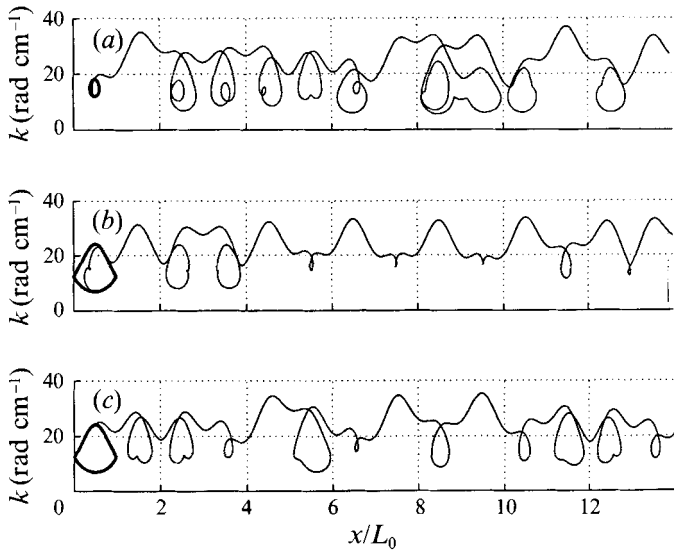

FIGURE 6. As figure 4(*c*) but with: (*a*) $k_0 = 12$ rad cm^{-1}, (*b*) $k_0 = 6.8377$ rad cm^{-1} and (*c*) $k_0 = 24.1491$ rad cm^{-1}. The heavy closed lines correspond to only one single long wave present.

wavelength, Klinke & Jähne (1992) found significant energy levels for waves of a few millimetres wavelength. Apparently, such very short waves can be maintained at some quasi-equilibrium state by the wind. Unfortunately, the observational results appear difficult to interpret in terms of an energy balance equation.

Trajectories similar to those of capillary–gravity waves over two short gravity waves can be found for 1 m wavelength gravity waves propagating in the field of two surface currents. Viscous dissipation is much less effective except in the case of a high β_i value (see figure 3*c*). In this case, the wave groups would break before the very high-wavenumber range is reached.

While the correct amplitude equations in these specific situations need still further – possibly very complicated – work, our first objective here is to look at the trajectories of the short waves in the presence of many surface flows of larger scales. In that respect, the analytical study which follows is concerned with a quite general problem.

4. Approximate analytical models

The examples treated numerically above give some insight into the effect of a second long wave on the trajectory of short-wave packets originally trapped in the trough of a first long wave. However, the numerical results are difficult to interpret in terms of simple physics. So it is of interest to develop models to look at general features of the trajectories, in the hope of achieving more insight.

The second-order equation for the dimensionless displacement $K_0 x$ can be derived from equation 15(*a*). No confusion being possible, this displacement will still be denoted as x. The equation is written

$$\ddot{x} = \frac{K_0}{4}\frac{\dot{k}}{k}\left(\frac{g}{k}+\gamma k\right)^{-3/2}\left[6\gamma g + 3(\gamma k)^2 - \left(\frac{g}{k}\right)^2\right]$$

$$- C_0 K_0 \beta_0 \dot{x}\sin x - CK_0\beta\left(\frac{K}{K_0}\dot{x}+\delta\Omega_0\right)\sin\left(\frac{K}{K_0}x+\delta\Omega_0 t+\psi\right). \quad (16)$$

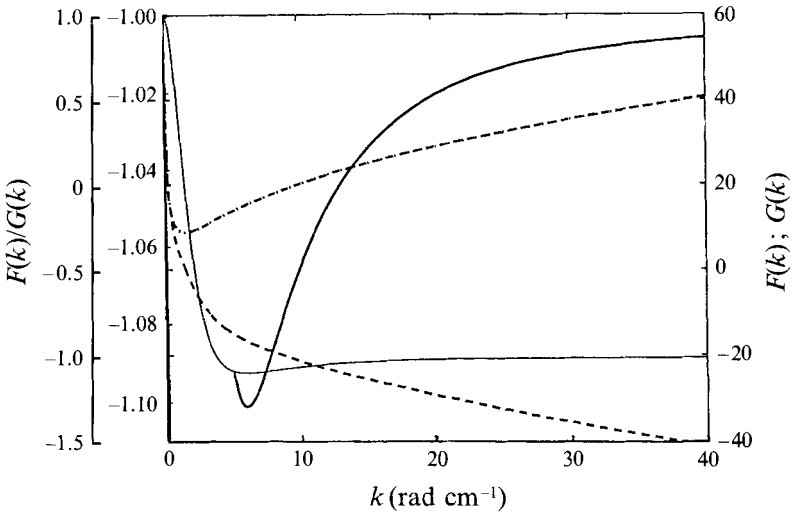

FIGURE 7. Variations with respect to the wavenumber k of $F(k)$ (–·–) and $G(k)$ (– –); $F(k)/G(k)$ is shown by a light line with external left ordinate for k from 0 to 40 rad cm^{-1}; heavy line with internal left ordinate for k from 5 to 40 rad cm^{-1}.

The next step is to eliminate k from this equation. This is strictly possible only if the surface tension effect is ignored. In that case, the first term of the equation becomes

$$G_g(k) = -\frac{K_0}{4}\frac{\dot{k}}{k}\left(\frac{g}{k}\right)^{1/2}, \tag{17}$$

where $(g/k)^{1/2}$ and $\dot{k}/k$ can be easily written in terms of x and t using (15).

With the surface tension terms, this procedure breaks down. To avoid lengthy and tedious algebra, an approximate procedure is used to eliminate k in (16). $\dot{k}/k$ can be evaluated at once in terms of x and t from 15(b). Then, an attempt was made to relate $(g/k+\gamma k)^{-3/2}[6\gamma k+3(\gamma k)^2-(g/k)^2]$ to the first term of 15(a). This was done by comparing the two functions

$$G(k) = \frac{1}{2}\left(\frac{g}{k}+\gamma k\right)^{1/2}\left(\frac{1}{2}+\frac{\gamma k}{g/k+\gamma k}\right) \tag{18a}$$

and

$$F(k) = -\frac{1}{4}\left(\frac{g}{k}+\gamma k\right)^{-3/2}\left[6\gamma k+3(\gamma k)^2-\left(\frac{g}{k}\right)^2\right]. \tag{18b}$$

They are displayed on figure 7 for k ranging from 0.01 to 40 rad cm^{-1}.

$G(k)$ can be written

$$G(k) = \frac{1}{4}\left(\frac{g}{k}+\gamma k\right)^{-3/2}[4\gamma g+3(\gamma k)^2+(g/k)^2] \tag{19}$$

so that

$$\frac{F(k)}{G(k)} = -\frac{6\gamma g+3(\gamma k)^2-(g/k)^2}{4\gamma g+3(\gamma k)^2+(g/k)^2}. \tag{20}$$

Figure 7 also displays this ratio in the same range of k. As expected, for small k (gravity range), the ratio tends to 1 while for high k, it tends to -1. Large variation is observed for k in the range 0.01 to about 5 rad cm^{-1}. As shown, above the latter value, the

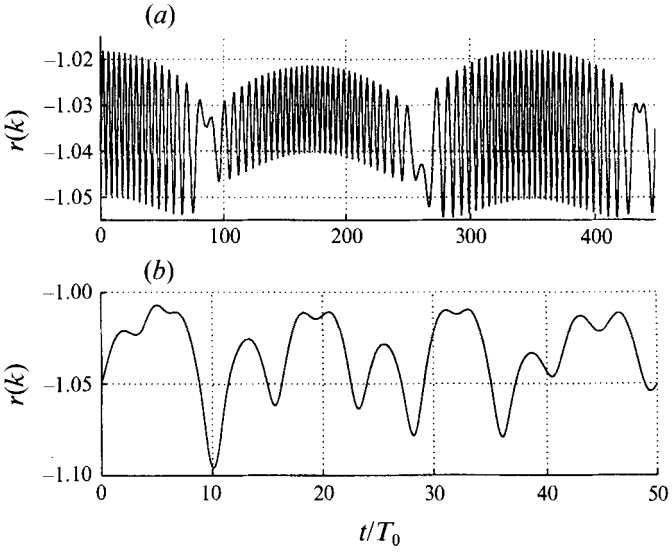

FIGURE 8. Time (t) evolution of $r(k) = F(k)/G(k)$ at initial wavenumber $k_0 = 12$ rad cm^{-1} in the presence of two long waves with (*a*) $\delta = 1/176$ and (*b*) $\delta = 1/7$.

ratio varies between about -1.1 and -1. To simplify the analysis, for k higher than 5 rad cm^{-1} the ratio will be taken as a constant, namely

$$F(k) \approx rG(k). \tag{21}$$

This procedure will be justified later on. Then,

$$\ddot{x} = -rK_0\frac{\dot{k}}{k}G(k) - \beta_0 C_0 K_0 \dot{x}\sin x - \beta CK_0\left(\frac{K}{K_0}\dot{x} + \delta\Omega_0\right)\sin\left(\frac{K}{K_0}x + \delta\Omega_0 t + \psi\right). \tag{22}$$

Using (15) to express $G(k)$ and $\dot{k}/k$ in terms of x, $\dot{x}$ and t yields

$$\begin{aligned}\ddot{x} = &-\beta_0\frac{r}{2}\Omega_0^2\sin x - \beta\Omega_0\Omega\left(\frac{r}{2} + \delta\frac{K_0}{K}\right)\sin\left(\frac{K}{K_0}x + \delta\Omega_0 t + \psi\right)\\ &-\left(1+\frac{r}{2}\right)\left[\beta_0\Omega_0\sin x + \beta\Omega\sin\left(\frac{K}{K_0}x + \delta\Omega_0 t + \psi\right)\right]\dot{x}\\ &+\frac{r}{2}\left[\beta_0\Omega_0\cos x + \beta\Omega\frac{K_0}{K}\cos\left(\frac{K}{K_0}x + \delta\Omega_0 t + \psi\right)\right]\\ &\times\left[\beta_0\Omega_0\sin x + \beta\Omega\sin\left(\frac{K}{K_0}x + \delta\Omega_0 t + \psi\right)\right],\end{aligned} \tag{23}$$

where $\Omega_0 = C_0 K_0$, $\Omega = CK$.

Under the above approximation of the first term of (16), equation (23) represents the general second-order equation which governs the displacement of a short-wave packet, with initially prescribed position and velocity, in the field of two longer gravity waves.

Before applying this equation to specific cases, we need first to justify (21). We recall that this is needed only for capillary–gravity waves. For pure gravity waves, (23) is exact with $r = 1$.

At a given initial value k_0 of k, the effect of the long waves is to produce variations of k and then of $r(k) = F(k)/G(k)$. Figure 8 displays such variations with

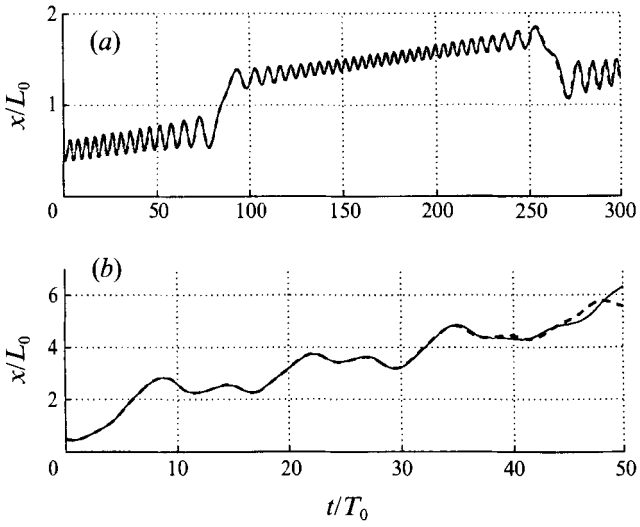

FIGURE 9. Comparisons between the time (t) evolution of short-wave displacements (with $k_0 = 12$ rad cm^{-1} and $x_0 = L_0/2$ in the field of two long waves with (a) $\delta = 1/176$ and (b) $\delta = 1/7$ as determined respectively from the exact system (15) (——) and the approximate equation (23) (– – –).

$k_0 = 12$ rad cm^{-1} and values of δ of 1/176 and 1/7. As expected, the extent of the variations is quite small. A natural choice of a constant approximate value for r is the mean value of the variations.

With the above values of δ, figure 9 shows a comparison between the displacements as determined by the exact system of equations (15) and by solving (23), r being taken as the mean value $\bar{r}$ of the variations above. It is seen that the respective displacements fit each other very well for a quite long time duration. As we will be mostly interested in displacements over a short time, the approximation is fully justifiable. Note that the determination of solutions to (22) needs the initial ($t = 0$) value of the position x_0 and the velocity $\dot{x}_0$. This velocity is given by

$$\dot{x}_0 = (g/k_0 + \gamma k_0)^{1/2}\left(\frac{1}{2} + \frac{\gamma k_0}{g/k_0 + \gamma k_0}\right) + \beta_0 C_0 \cos x_0 + \beta C \cos P - C_0, \tag{24}$$

with $P = (K/K_0)\,x + \delta\Omega_0 t + \psi$.

Three terms can be identified on the right-hand side of (23), namely

$$S_1 = -\beta_0 \frac{\bar{r}}{2}\Omega_0^2 \sin x - \beta\Omega_0\Omega\left(\frac{r}{2} + \delta\frac{K_0}{K}\right)\sin P, \tag{25a}$$

$$S_2 = -\left(1 + \frac{\bar{r}}{2}\right)\dot{x}[\beta_0\Omega_0 \sin x + \beta\Omega \sin P], \tag{25b}$$

and

$$S_3 = \frac{\bar{r}}{2}\left[\beta_0\Omega_0 \cos x + \beta\Omega\frac{K_0}{K}\cos P\right][\beta_0\Omega_0 \sin x + \beta\Omega \sin P]. \tag{25c}$$

The relative importance of these terms on the displacements was studied numerically. It was found that S_2 is much less important than the other two. The reason for this was not investigated further.

Here, we are mostly interested in the influence of a second long wave on the displacement of short-wave packets initially strongly trapped in the trough of a first

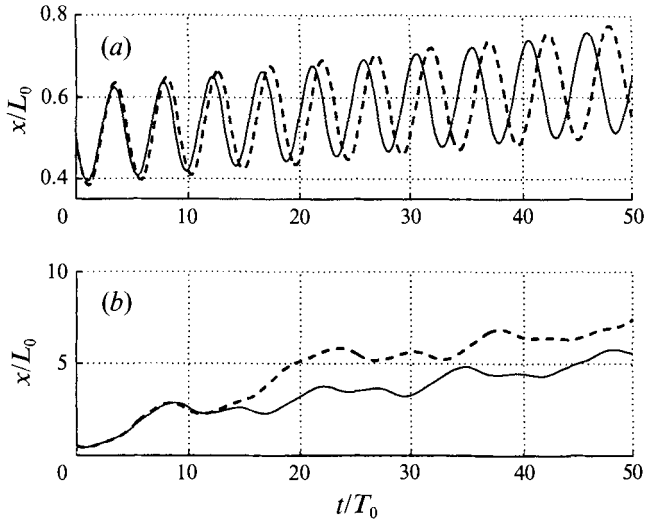

FIGURE 10. As figure 9 except that equation (23) is replaced by (26).

long wave. For such short waves, the displacement x and the velocity $\dot{x}$ would be small during a short time interval. More precisely, $x \ll 1$, while $\dot{x}$ will be of order $\beta_0 \Omega_0$.

First, retaining terms of order β_0 and β, the right-hand side of (23) reduces to S_1:

$$\ddot{x} \approx -\beta_0 \frac{\bar{r}}{2} \Omega_0^2 \sin x - \beta \Omega_0 \Omega \left(\frac{\bar{r}}{2} + \frac{\delta}{\alpha} \right) \sin (\alpha x + \delta \Omega_0 t + \psi), \tag{26}$$

with $\alpha = K/K_0$.

The validity of this equation was tested by comparison with the result of the exact system of equations (15). Figure 10 illustrates the comparison, again at $k_0 = 12$ rad cm^{-1} and $\delta = 1/176$ and $1/7$.

Up to about $t = 10T_0$ equation (26) predicts well the short-wave-packet displacement. This was confirmed at other values of δ. At larger time, (26) overestimates the displacements which, in addition, are more and more phase shifted with respect to the exact solution.

Next, we are interested in short-wave packets which exhibit a small displacement around their initial position x_0. Changing the variable to

$$\tilde{x} = x - x_0, \tag{27}$$

equation (26) becomes

$$\ddot{\tilde{x}} = -\beta_0 \frac{\bar{r}}{2} \Omega_0^2 \sin (\tilde{x} + x_0) - \beta \Omega_0 \Omega \left(\frac{\bar{r}}{2} + \frac{\delta}{\alpha} \right) \sin [\alpha(\tilde{x} + x_0) + \delta \Omega_0 t + \psi]. \tag{28}$$

With $\tilde{x} \ll 1$; $\sin \tilde{x} = \tilde{x}$; $\sin \alpha \tilde{x} \approx \alpha \tilde{x}$, $\cos \tilde{x} \approx \cos \alpha \tilde{x} \approx 1$, equation (28) reduces to

$$\ddot{\tilde{x}} + \left[\beta_0 \frac{\bar{r}}{2} \Omega_0^2 \cos x_0 + \alpha \beta \Omega_0 \Omega \left(\frac{\bar{r}}{2} + \frac{\delta}{\alpha} \right) \cos (\alpha x_0 + \delta \Omega_0 t + \psi) \right] \tilde{x}$$

$$= -\beta_0 \frac{\bar{r}}{2} \Omega_0^2 \sin x_0 - \beta \Omega_0 \Omega \left(\frac{\bar{r}}{2} + \frac{\delta}{\alpha} \right) \sin (\alpha x_0 + \delta \Omega_0 t + \psi). \tag{29}$$

Defining the variable τ by

$$2\tau = \pi - \alpha x_0 - \psi - \delta \Omega_0 t$$

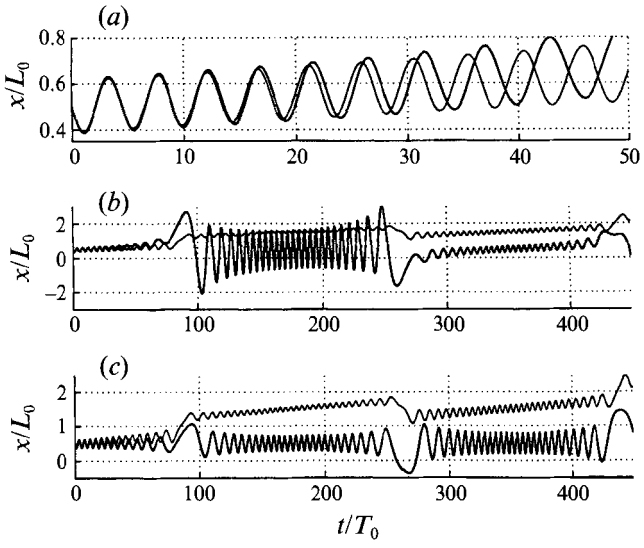

FIGURE 11. As figure 9(*a*) for $\delta = 1/176$ except that (23) is replaced by: (*a*, *b*), the inhomogeneous Mathieu equation (30) (heavy lines); (*c*) the homogeneous Mathieu equation (30) without the forcing term) (heavy line). The lighter lines are the exact solution, (15).

we have
$$\frac{\mathrm{d}^2}{\mathrm{d}\tau^2} = \left(\frac{2}{\delta\Omega_0}\right)^2 \frac{\mathrm{d}^2}{\mathrm{d}t^2}$$

and
$$\sin 2\tau = \sin(\alpha x_0 + \delta\Omega_0 t + \psi), \quad \cos 2\tau = -\cos(\alpha x_0 + \delta\Omega_0 t + \psi).$$

Simple algebra yields
$$\frac{\mathrm{d}^2\tilde{x}}{\mathrm{d}\tau^2} + (a - b\cos 2\tau)\,\tilde{x} = -(c + b'\sin 2\tau), \tag{30}$$

with
$$a = \beta_0 \frac{\bar{r}}{2}\left(\frac{2}{\delta}\frac{\Omega_0}{\Omega_0}\right)^2 \cos x_0, \quad b = \alpha\beta\frac{\Omega_0}{\Omega}\left(\frac{2}{\delta}\frac{\Omega}{\Omega_0}\right)^2\left(\frac{\bar{r}}{2} + \frac{\delta}{\alpha}\right),$$

$$c = \beta_0 \frac{\bar{r}}{2}\left(\frac{2}{\delta}\frac{\Omega_0}{\Omega_0}\right)^2 \sin x_0, \quad b' = b/\alpha.$$

We recognize equation (30) as a Mathieu equation with a forcing term.

Figures 11 and 12 illustrate the results of a preliminary investigation based on equation (30), again with $\delta = 1/176$ and $1/7$. As in the previous examples, $k_0 = 12$ rad cm^{-1}. With $\delta = 1/176$, as shown on figure 11(*a*), the short-wave displacement predicted by (30) fits well the displacement computed from the exact system (15) up to values of t/T_0 of order 20. Surprisingly, for a short time interval, (30) appears a better approximation than (26) (see figure 10*a*). However, at larger time, (30) overestimates the displacement more than equation (26).

With $\delta \approx 1/176$, a is clearly much larger than unity and b is of order a. This is the well-known case where the WKB approximation applies (see e.g. Morse & Feshbach 1953).

The approximate solution to (30) is
$$\eta = \frac{A}{\omega^{1/2}}\sin\left(a^{1/2}\int_0^t \omega\,\mathrm{d}\tau\right) + \frac{B}{\omega^{1/2}}\cos\left(a^{1/2}\int_0^t \omega\,\mathrm{d}\tau\right) - \frac{b'}{a\omega^2}\sin 2\tau, \tag{31}$$

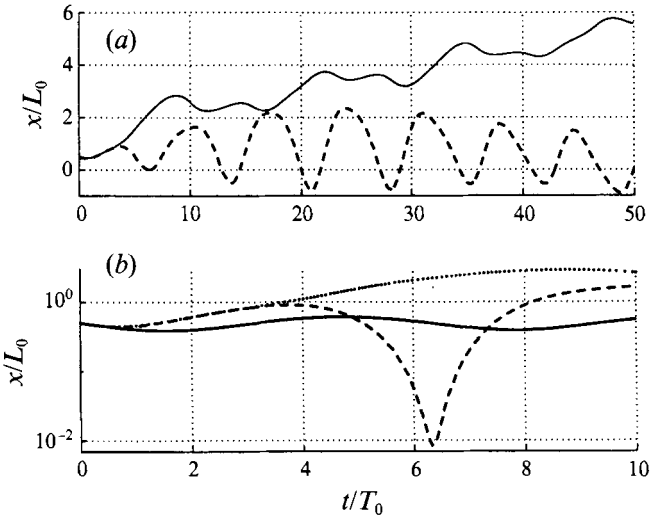

FIGURE 12. (*a*) As figure 9(*b*) for $\delta = 1/7$ except that (23) is replaced by (30); (*b*) ——, only the first long wave present, ..., solution to the exact system (15).

with $$\omega(\tau) = (1 - b/a\cos 2\tau)^{1/2}. \tag{32}$$

From the physical viewpoint, the approximation corresponds to an autocorrelation period much larger than the basic period T_0. The two first terms of (31) mean that the short-wave packet moves back and forth many times in the trough of the long waves which evolve slowly. With $b \approx a$, the frequency ω approaches zero at each autocorrelation cycle, and the short-wave packet would escape blockage at each cycle. As shown in figure 11(*b*), the solution of (30) confirms the above prediction of the WKB solution, namely that the displacement exhibits cycles governed by the autocorrelation time. As expected from (31), the driving term in (30) would not influence the cycle timescale. This is confirmed by figure 11(*c*) which shows the solution of the homogeneous form of (30). In fact, the forcing term in this equation, which corresponds to the third term in (31), is responsible for the slow drift of the mean displacement of the short-wave packet within each cycle. The mean displacement then moves away from the initial position. At the end of each cycle, the short wave may temporarily leave the initial long-wave trough but will rapidly come back to this location. This happens for the homogeneous equation as well.

Finally, the homogeneous and the forced Mathieu equation cannot predict one of the main features of the short-wave displacement as given by the exact solution, namely that the short-wave packet can effectively leave the initial long-wave trough to jump to other troughs. The jumps are clearly due to nonlinear effects and were also found in the solutions of (26).

With $\delta = 1/7$, equation (30) again predicts well the displacement for a short time interval (figure 12*a*). The following remark could be of interest: as shown on figure 12(*b*), up to the reflection point (see figure 5*b*) the second wave does not play a significant role, but once this point is reached, the displacement has a tendency to exhibit an exponential evolution. This is true for the exact displacement (equation (15)) as well as for the approximate result from equation (30). Then, as seen in figure 12(*a*) the short wave jumps to the next basic long-wave trough. Again, this large displacement cannot be predicted by the Mathieu equation and is clearly due to nonlinear effects in the exact solution. As a result the short wave becomes rapidly untrapped.

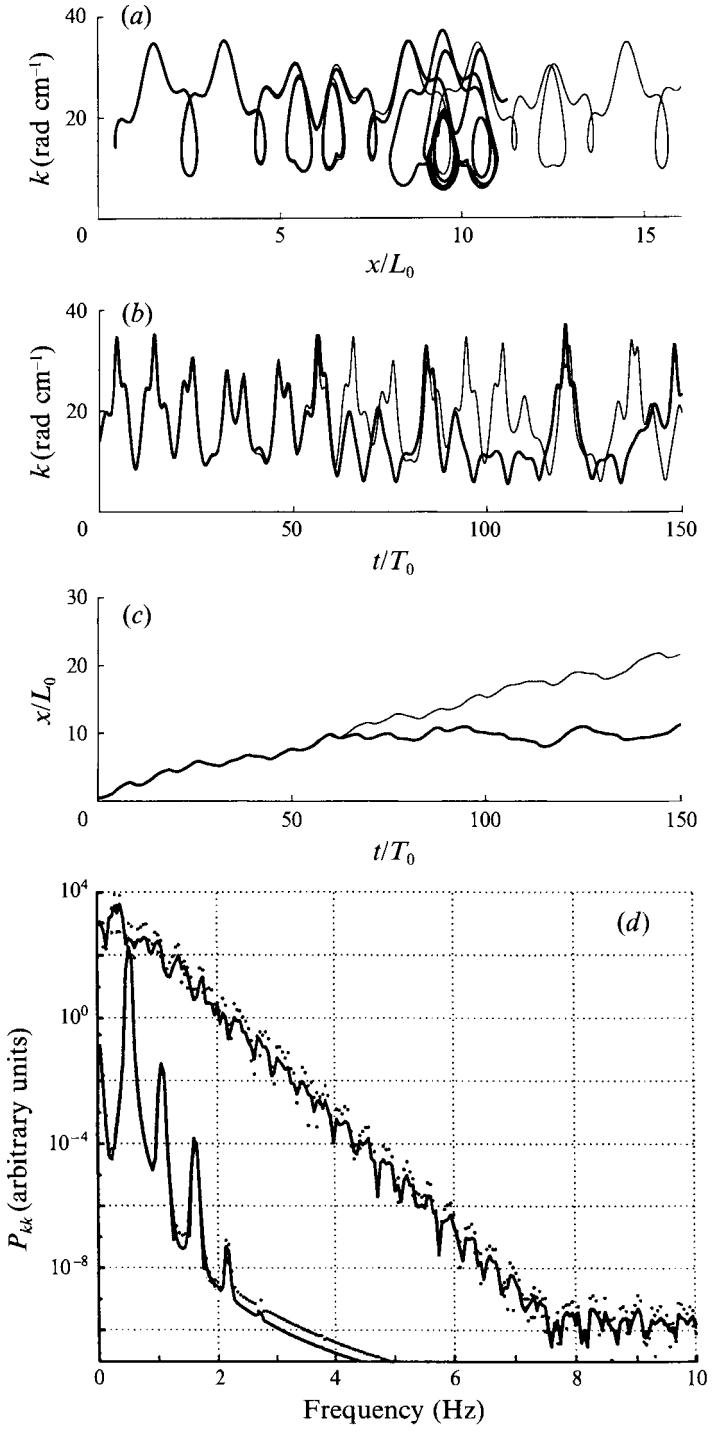

FIGURE 13. Short-wave trajectories in WKB phase space (*a*) and time evolutions of the wavenumber (*b*) and the position (*c*) corresponding to two slightly different initial conditions: $k_0 = 14$ rad cm^{-1}, $x_0 = L_0/2$ (light lines); $k_0 = 14+0.01$ rad cm^{-1}, $x_0 = L_0/2+0.01$ (heavy lines). (*d*) Frequency spectrum of the wavenumber variations with $k_0 = 14$ rad cm^{-1}, in the presence of a single long wave (lower curve) and in the presence of two long waves (upper curve $\delta = 1/7$); the dots display the 95% confidence intervals.

Finally it may be of interest to note that, at large time, the trajectories shown in figures 5 and 6 suggest some chaotic regime such as described by Thompson & Stewart (1986): 'certain patterns in the waveform repeat themselves at irregular intervals, but there is never exact repetition'.

The existence of such a regime is better illustrated in figure 13 which shows trajectories and time evolutions of the wavenumber and the position corresponding to slightly different initial conditions. It is seen that the trajectories remain close to each other for some time and then diverge rapidly to become uncorrelated. This occurs for the time evolutions as well. In addition, as shown on figure 13(*d*), in the presence of a single long wave, the frequency spectrum of the wavenumber variations is discrete, consistent with their periodic feature. With a second long wave present, the spectrum becomes continuous. This also suggests a chaotic regime.

The detailed examination of this regime, which would include in particular Poincaré maps, is beyond the scope of this first work but would be of great interest. Much effort could be devoted to the physical interpretation of the expected results of such an investigation.

5. Concluding remarks

This work constitutes a first step in investigations concerning the dynamics of short surface waves propagating over a large-scale surface velocity field in the realistic case where this field contains many harmonic components. The work is limited to the kinematic aspect. While specific examples are treated, the results would be of general interest as partially proved by the similarity of results found for capillary–gravity waves over long gravity wave and for 1 m wavelength range gravity waves over a surface current related to internal waves. The fact that a driven Mathieu equation governs the short-wave displacement at a short time interval is also of general importance and will be exploited in future work.

The main result of the investigation is that the presence of a second surface velocity field can strongly modify the trajectories of the short-wave packets from what happens in the presence of only one single field. In particular, short waves well trapped by this field become untrapped within some time interval. The parameter controlling this interval is clearly identified.

Other results, not reported here, show that the short-wave packets can be removed from blockage by nonlinear dispersion or the presence of other short waves. Also, variability in the phase ψ (see (16)) produces the same effect.

The case of many (more than two) large-scale surface velocity fields, eventually random, is of course of crucial interest in practice, but probably very difficult to handle. As far as the blockage process is concerned, the spectral bandwidth of the velocity variations would be the generalization of the parameter δ above: for narrow bandwidth, temporary blockage would occur while for wide bandwidth, free propagation of the short waves would be expected. The latter situation would occur often in natural conditions where the short waves suffer the joint effects of the dominant long waves and surface currents at much larger characteristic scales than these dominant waves.

From the observational viewpoint, temporary blockage of capillary or capillary–gravity waves at fixed phase of the dominant gravity waves is commonly visually observed in laboratory facilities. After a certain time, these short waves are removed from blockage. This may be related to the present analysis as the dominant wave can be, to first approximation, considered as a modulated wavetrain. But other effects such

as nonlinear dispersion may be involved. The important fact is the existence of a local and instantaneous dispersion which is generally not accounted for in most experimental and theoretical studies of water surface waves. Strictly, the shorter surface wave fields become multidispersive so that the interpretation of experimental results on the dispersion relation may be very ambiguous as the spatio-temporal variations are ignored.

Finally, the existence of local and instantaneous dispersion may be of interest in studying some intermittent events occurring in the short surface wave fields. A typical example is the collectivization of short waves trapped at a certain phase of the surface velocity field variations. If nonlinear effects are considered, this would lead to important consequences due to short-wave interactions.

The obvious general problem to be considered in future works deals with the dispersion of an ensemble of short waves in the presence of an ensemble of surface flows of larger scales. Three-dimensional effects as well as the amplitude evolution would need to be included. This clearly constitutes a formidable task which will possibly need many steps of investigation. Short waves generated by the wind are of main interest in practice. But then a particular difficulty arises as the amplitude equation is still the subject of a large controversy.

The simple examples treated here illustrate the important effects of the unsteadiness in the dispersion of the short waves and possibly in their dynamical evolution in general. Such effects may be missed by simply looking at averaged properties. From the experimental viewpoint, extensive use of the recently developed methods to process unsteady or non-stationary data would reveal new fundamental aspects of the physics of surface waves. First applications of such methods (Chapron & Ramamonjiarisoa 1992; Ramamonjiarisoa, Chapron & Branger 1993) indeed show the presence of striking transient mechanisms.

The author is indebted to Dr Erik Mollo-Christensen for his invaluable help in improving a first draft manuscript of this paper. It is also a pleasure to acknowledge Dr O. M. Phillips for helpful discussions on the subject. Many comments and suggestions of the referees about various aspects of the paper are greatly appreciated.

REFERENCES

BASOVICH, A. Y. 1979 Transformation of the surface wave spectrum due to the action of an internal wave. *Izv. Atmos. Ocean Phys.* **15**, 448–452.

BASOVICH, A. Y. & BAHANOV, V. V. 1984 Surface wave kinematics in the field of an internal wave. *Iz. Atmos. Ocean. Phys.* **20**, 50–54.

BASOVICH, A. Y. & TALANOV, V. I. 1977 Transformation of short surface waves on inhomogeneous currents. *Izv. Atmos. Ocean. Phys.* **13**, 514–519.

BRETHERTON, F. P. & GARRETT, C. J. R. 1968 Wavetrains in inhomogeneous moving media. *Proc. R. Soc. Lond.* A **302**, 529–554.

CHAPRON, B. & RAMAMONJIARISOA, A. 1992 Observations of the evolution of nonlinear deep-water gravity waves. In *Proc. Nonlinear Water Waves Workshop, University of Bristol* (ed. D. H. Peregrine).

GASPAROVIC, R. F., APEL, J. R. & KASISCHKE, E. S. 1988 An overview of the SAR internal wave signature experiment. *J. Geophys. Res.* **93** (C10), 12304–12316.

HENYEY, F. S., CREAMER, D. B., DYSTHE, K. B., SCHULTZ, R. L. & WRIGHT, J. A. 1988 The energy and action of small waves riding on large waves. *J. Fluid Mech.* **189**, 443–462.

IRVINE, D. E. 1987 Extreme waves in the Agulhas. A case study in wave-current interaction. *Johns Hopkins APL, Tech. Digest.* vol. 8 (1), pp. 100–106.

KLINKE, J. & JÄHNE, B. 1992 2D wave number spectra of short wind waves. Results from wind wave facilities and extrapolation to the ocean. In *Optics of the Air-Sea Interface: Theory and Measurements* SPIE Proc., vol. 1749.

LONGUET-HIGGINS, M. S. & STEWART, R. W. 1960 Changes in the form of short gravity waves on long waves and tidal currents. *J. Fluid Mech.* **8**, 565–583.

LONGUET-HIGGINS, M. S. & STEWART, R. W. 1961 The changes in amplitude of short gravity waves on steady non-uniform currents. *J. Fluid Mech.* **10**, 529–549.

MELVILLE, W. K. & RAPP, R. J. 1988 The surface velocity field in step and breaking waves. *J. Fluid Mech.* **189**, 1–22.

MORSE, L. M. & FESHBACH, H. 1953 *Methods of Theoretical Physics.* McGraw-Hill.

PHILLIPS, O. M. 1977 *The Dynamics of the Upper Ocean*, 2nd edn. Cambridge University Press.

PHILLIPS, O. M. 1981 The dispersion of short wavelets in the presence of a dominant long wave. *J. Fluid Mech.* **107**, 465–485.

RAMAMONJIARISOA, A., CHAPRON, B. & BRANGER, H. 1993 Analysis par traitements temps-echelles et methodes adaptatives des evolutions non linéaires d'ondes de surface. In *Proc. 14th GRETSI Colloquim on Data and Images Processings,* pp. 1371–1374.

SHYU, J. H. & PHILLIPS, O. M. 1990 The blockage of gravity and capillary waves by longer waves and currents. *J. Fluid Mech.* **217**, 115–141.

SINITSYN, YU. A., LEYKIN, I. A. & ROZENBERG, A. D. 1973 The space-time characteristics of ripple in the presence of long waves. *Izv. Atmos. Ocean. Phys.* **9**, 511–519.

THOMPSON, J. M. T. & STEWART, H. B. 1986 *Nonlinear Dynamics and Chaos.* John Wiley.

TRULSEN, K. & MEI, C. C. 1993 Double reflection of capillary–gravity waves by a non-uniform current: a boundary-layer theory. *J. Fluid Mech.* **251**, 271.